Mineralogy and Petrology
https://doi.org/10.1007/s00710-026-00993-x

RESEARCH

Petrogenesis of isolated high-silica rhyolites in Iceland

Amanda L. Hughes[1,2] · Joaquín A. Cortés[2] · Dave McGarvie[3] · Hugh Tuffen[3] · Kristján Jónasson[4] · Andrew G. Tindle[5]

Received: 25 October 2024 / Accepted: 17 April 2026

Abstract

High-silica rhyolites (HSRs) are rhyolites containing > 75 wt% SiO_2 on an anhydrous basis. In this contribution we have studied four Icelandic isolated occurrences away from central volcanoes (i.e., Icelandic volcanoes with a well-developed volcanic plumbing system): three in active rift zones (Mælifell, Ketilhyrnur and Prestahnúkur) and one in a flank/off-rift zone (Sultarfell). With no established central volcano, in which magmas can evolve by fractional crystallisation in its plumbing system, we propose that these high-silica volcanic rocks are the product of partial melting of tonalitic Icelandic crust (i.e., plagiogranites). We have modelled their petrogenesis using alphaMELTS (a command line frontend of rhyolite-MELTS), first involving fractional crystallisation from a mantle-derived basaltic melt to generate the plagiogranite, and then partial melting of plagiogranites at shallow depths (~4 km), compatible with a pressure range constrained by the haplogranite system minima. Rayleigh and batch melting models are consistent with this method, fairly reproducing some of the incompatible trace elements compositions found in the HSR occurrences (e.g., Y and Rb ~ 100 ppm), but failing to reproduce others (e.g., Zr < 400 ppm and Nb < 60). This inconsistency however supports the proposed partial melting model, in which zircon and ilmenite, found in plagiogranites, remain in a refractory restite. A partial melting model also supports unusual assemblages found in Prestahnúkur samples, comprising allanite, zircon, fayalite, hedenbergite, and ilmenite, along with an intermediate plagioclase and quartz. The discrepancy between the mineral chemistry of these phases and the expected compositions according to the modelling suggest that some of this mineralogy is likely to be xenocrystic, with mineral phases such as zircon being derived directly from underlying plagiogranites.

Keywords High silica rhyolites · alphaMELTS · Rhyolite-MELTS · Plagiogranite · Iceland · Allanite

Introduction

High-silica rhyolites (HSRs) are volcanic rocks containing over 75 wt% of SiO_2 on an anhydrous basis (MacDonald et al. 1987; Streck and Grunder 1997; Gualda and Ghiorso 2013; Wolff and Ramos 2015; Zincone et al. 2016; Zhang et al. 2018). Although they are relatively uncommon, they occur in all tectonic settings on Earth: i.e., in subduction zones (e.g., Rattlesnake Tuff, back-arc of the Cascades volcanic range; Streck and Grunder 1997), rift zones (e.g., in the Kenyan rift valley; MacDonald et al. 1987), and in intraplate settings (e.g., Bandelier tuff, New Mexico; Wolff and Ramos 2015). Regardless of the setting, HSRs typically occur as holohyaline domes and coulées (Bacon et al. 1981; Lee and Morton 2015). Petrogenetically, they have been modelled as products of extreme magma evolution by fractional crystallisation (e.g., Miller and Mittlefehldt 1984; Glazner et al. 2008), partial melting of various lithologies (Lowenstern and Mahood 1991; Deering et al. 2008; Lee

Editorial handling: M. Grazia Perna

✉ Amanda L. Hughes
A.L.Hughes@ljmu.ac.uk

[1] Department of History, Geography and Social Sciences, Edge Hill University, Ormskirk L39 4QP, UK

[2] Department of Health, Innovation, Technology and Science, John Moores University, Liverpool L3 2AJ, UK

[3] Lancaster Environment Centre, Lancaster University, Lancaster LA1 4YQ, UK

[4] Natural Science Institute of Iceland, Urridaholtsstraeti 6-8, 210 Gardabaer, Iceland

[5] Milton Keynes, UK

Published online: 03 July 2026

and Morton 2015) or a combination of both processes (e.g., Gurenko and Sobolev 2006; Martin and Sigmarsson 2007).

Fractional crystallisation may be expected to generate a compositional continuum from silica-poorer "regular" rhyolites (hereafter termed rhyolites) to HSRs; however, this is not always the case. At a given constant pressure, silica content can only increase by fractional crystallisation until an invariant (minimum/eutectic) point is attained, stopping silica concentration increasing in the melt after further fractionation (Blundy and Cashman 2001; Gualda and Ghiorso 2013). For example, at pressures of ~ 1 GPa that value is around 74 wt% SiO_2. Higher silica concentrations can be achieved by melt decompression to shallower depths.

Additionally, further crystallisation and removal of any mineral phase from evolved melts does not play a relevant role in rhyolite petrogenesis, as these melts typically have low nucleation rates inhibiting crystallisation (e.g., Kirkpatrick 1983), and their high viscosity hinders fractionation (Bowen 1921). Models involving the removal of interstitial melt within a crystal mush are usually invoked instead of standard fractional crystallisation (Bachmann and Bergantz 2004; Lee and Morton 2015), again with the silica content of the resultant melt constrained by the eutectic/minimum (e.g., Blundy and Cashman 2001), the pressure, and the melt's volatile content (e.g., H_2O, F, B). In particular, fluorine, boron, and phosphorus in conjunction with water, substantially decrease the viscosity of a granitic melt, enhancing its potential removal (Bartels et al. 2013).

Thus, HSRs are the products of the extreme evolution of magmatic systems, in some cases up to 90% fractional crystallisation starting from a basaltic magma (Miller and Mittlefehldt 1984) involving decompression-driven crystallisation during evolution (Gualda and Ghiorso 2013) or they are the consequence of a two-stage process (e.g., Bacon et al. 1981; Deering et al. 2008). Alternatively, HSRs may be derived by partial melting of the crust, constrained by the minimum of the haplogranite cotectic at shallower depths (> 300 MPa) than rhyolites (Gualda and Ghiorso 2013). In this work we explore the occurrence of isolated HSRs in Iceland, and how these models can be adapted to an Icelandic specific context.

High-silica rhyolites in Iceland

Volcanism in Iceland is the consequence of the rifting of the North Atlantic and Eurasian plates and decompression of the lithospheric mantle, in conjunction with a thermal anomaly likely associated to a mantle plume, which coupled with the spreading centre at ~ 25 Ma (Lawver and Müller 1994). Although basalts dominate both intrusive and eruptive sequences, *Central Volcanoes* (hereafter CVs), which in Iceland are volcanoes having a well-defined crustal magma reservoir and volcanic plumbing (e.g., Thordarson and Larsen 2007) have long been recognised as mostly bimodal, basalt – rhyolite systems (e.g., Bunsen 1851; Walker 1966). Previous studies (e.g., Jónasson 2007; Thordarson and Larsen 2007) have estimated 79–83 vol% of associated basalts with 10–15% of rhyolites, in contrast with ~ 8 vol% of andesites and dacites. Regardless of this strong bimodality, fractional crystallisation has been traditionally proposed by many authors as the main mechanism to generate evolved rocks in Iceland (Carmichael 1964, and references therein).

It is then generally accepted that CV rhyolites are linked to long-lived trans-crustal magma systems in which mainly fractional crystallisation occurs in the shallow regions of the plumbing system (e.g., Gurenko and Sobolev 2006; Martin and Sigmarsson 2007; Thordarson and Larsen 2007). Other processes such as partial melting, contamination/assimilation of crust, magma mixing and hydrothermal alteration could also occur and generate rhyolites, driven by the thermal energy derived from basaltic melts generated by partial melting in the mantle (Gudmundsson 1995). Irrespective of whichever process dominates, a key CV feature is that the occurring rhyolites are most of the time genetically related to the basalts (e.g., Lacasse et al. 2007). Thus, in rift zones CVs, tholeiitic basalts are typically related to sub-alkaline rhyolites, whereas in flank zones CVs transitional alkali basalts are associated to alkaline rhyolites (in the sense of Irvine and Baragar 1971, and references therein).

There are few documented occurrences of HSRs at Icelandic CVs, most notably are the near-aphyric HSR magmas at Krafla, sampled at the surface (Jónasson et al. 1992; Tuffen and Castro 2009); at Þingmúli volcano (Carmichael 1964; Hughes et al. 2026); and extracted from 2.1 km depth by the IDDP-1 borehole in 2009 (Elders et al. 2011; Masotta et al. 2018; Saubin et al. 2021). The compositions (major and trace elements) of the Krafla HSRs were successfully reproduced by variable degree of partial melting experiments, starting from a Krafla rhyolite and a felsite (Masotta el at. 2018). At Þingmúli volcano, HSRs are not genetically related to its basalts, and they have been modelled as generated by partial melting of underlying rhyolitic ignimbrites originated from the nearby Reyðarfjörður central volcano (Hughes et al. 2026). Hydrogen isotopes and water concentrations in IDDP-1 glasses further point towards their origin from variable degrees of partial melting of a felsite in the presence of a hydrous fluid of mixed meteoric and magmatic origin (Saubin et al. 2021). Partial melting seems to be a common feature in the petrogenesis of HSRs associated to CVs, as these typically have associated well-established plumbing systems with long-lived hydrothermal convective cells (e.g., Streck 2002).

In this work we study Icelandic HSRs that are not associated with CVs and their long-established plumbing system,

as no past study has reviewed their chemical characteristics, and likely petrogenesis.

HSRs occurrences

Here, we examine the geochemistry and petrogenesis of four occurrences of isolated HSRs: Prestahnúkur, Mælifell, Ketilhyrnur, and Sultarfell. The first three occur in active rift zones, while Sultarfell occurs in a flank (non-rifting) zone in southern Iceland (Fig. 1). All four occurrences are small in volume, and are not associated with any CV. They are all subglacial rhyolite outcrops, varying in volume from 0.05 to 1.6 km^3 (total volume ~ 3 km^3), with Prestahnúkur the largest. Field evidence suggests that each of the four HSR occurrences are the product of single, effusive eruptions. McGarvie et al. (2007) analysed six samples from Prestahnúkur, specifically to test whether one or more magma batches were involved, and concluded that the lack of compositional variation (especially trace elements), indicated the involvement of only one magma batch. Only one of the four occurrences has been dated (Prestahnúkur), with an imprecise Ar–Ar age of 89 ± 24 ka (McGarvie et al. 2007).

Methods

Sampling, petrography and glass/mineral chemistry

Samples were collected by D. McGarvie during fieldwork in Iceland in 1999 (Prestahnúkur and Maelifell), in 2000 (Ketilhyrnur), and in 2014 by D. McGarvie and J. Moles (Sultarfell). Sample size was generally a minimum of 12 × 8 × 8 cm. For Icelandic rhyolites that are largely aphyric or microcrystalline and contain a small percentage of microphenocrysts (i.e. less than 5% by volume), a sample size of 3 × 3 × 3 cm is sufficient to provide representative major and trace element geochemistry (e.g., MacDonald et al. 1990; McGarvie et al. 1990). For petrography, the selected samples were cut with a diamond edge saw and lapped on a Struers Labopol rotating horizontal plate to diamond grid grades of 150 µm and 63 µm to remove any surface irregularities. Similar procedure was done on 75 × 25 mm glasses using a 30 µm carborundum grit (silicon carbide and water). The grinded rock slabs were then glued into the glass using the epoxy resin Araldite in a 10:1 ratio with hardener and reduced until a thickness of 30 µm with the carborundum grit. Samples for standard petrography were covered with a protective glass slab and uncovered, double polished and carbon-coated for microprobe analyses.

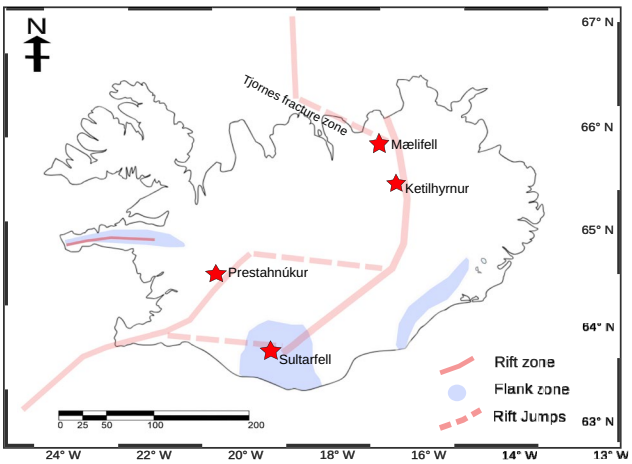

Fig. 1 Locations of the four HSR studied in this work: Prestahnúkur, Sultarfell, Mælifell and Ketilhyrnur (red stars). Also shown are both rift (pink lines) and flank (solid blue areas) zones in Iceland. Red dashed lines indicate 'rift jumps' and the Tjornes fracture zone (after Einarsson and Sæmundsson 1987)

Chemistry of glasses and mineral crystalline phases were determined on double polished carbon-coated thin sections, using the CAMECA SX100 electron microprobe at The Open University (UK) operating in wavelength-dispersion mode. The system is equipped with five wavelength-dispersive X-ray spectrometers with LTAP, PET, TAP, LPET and LLIF crystals and a single energy-dispersive X-ray spectrometer and both secondary and backscattered detectors. We used a combination of standard reference materials, including minerals (baryte, bustamite, cobaltite, crocoite, hematite, stibnite, willemite), pure metal (Cu, Ag, V, Ni) and synthetic standards (Cr_2O_3, KCl, LiF), and the following X-ray lines: synthetic LiF (FKα), jadeite (NaKα and AlKα), forsterite (MgKα), feldspar (AlKα, SiKα and KKα), synthetic KCl (ClKα), rutile (TiKα), bustamite (MnKα and CaKα), hematite (FeKα), and willemite (ZnKα). Additionally, to check the accuracy and precision of the EPMA, and to monitor any drift in the instrument (Meek et al. 2012), repeat analyses of a secondary standard, the Corning B glass (Brill 1999), were included at the start and finish of each analytical run. An operating voltage of 20 kV and probe current of 20 nA (measured on a Faraday cage) were used. The diameter of the beam was 10 µm. Count times varied from 20 to 80 s per element, and data were corrected using a PAP correction procedure (Pouchou and Pichoir 1991). The analytical set-up for quantitative compositional analyses was as follows: 20 kV accelerating voltage, a 20 nA beam current and a 25 µm defocused beam. The counting times were between 10 and 40 s on the peak and 15 s on the background either side of the peak. A defocused beam was used to minimise the effect of the migration of alkalis (e.g. Na_2O) from the samples (Henderson 1988).

Lower limits of detection (LLDs) for electron microprobe analyses were estimated from counting statistics under the same analytical conditions as the unknowns, using background measurements acquired for each element. LLDs were calculated as three times the standard deviation of the background count rates and converted to concentration using matrix-matched standards and PAP corrections.

Bulk whole-rock geochemistry

Whole-rock major and trace element compositions (Table 1) were determined by X-ray fluorescence spectrometry at The Open University (Mælifell, Ketilhyrnur and Prestahnúkur) and at the University of Leicester (Sultarfell), using the Thermo SCientific ARL 8420 + dual goniometer wavelength dispersive XRF spectrometer (The Open University), and a PANalytical Axios Advanced XRF Spectrometer (University of Leicester).

For both instruments, samples were split and crushed using a hydraulic splitter and a jaw mill. Fragments of 2–3 mm where grinded using a tungsten carbide rings apparatus (The Open University) or using agate balls (4–5 balls 20 mm diameter) apparatus (Leicester). In both labs, sample powders were left in a desiccator at 105–110°C for 24 h. Major-element concentrations were then measured on 40 mm-diameter fused glass discs. About 0.9 g of sample powder was mixed with a borate flux using a 5:1 (flux: sample) dilution and fused in Pt-5%Au crucibles at 1100°C. Trace elements were determined on pressed powder pellets made with 9 g of powder mixed with few drops of a Mowiol 4–88 solution (Leicester) and pressed on a hydraulic press.

Loss on ignition (LOI), was determined by heating ~ 1 g of sample material to 900-1050 °C for 1.5–2 h (Open University) or at 950 °C for 1 to 1.5 h (Leicester) and is the total effect of dehydration (loss of weight) and oxidation of ferrous iron (gain of weight). As standards, the Rhyolite Glass Mountain 1 (RGM-1) from the USGS (Gladney and Roelandts 1988) was used at The Open University, while basalt BHVO-1 (Gladney and Roelandts 1988), Gabbro MRG-1 (Gladney and Roelandts 1990) and peridotite JP-1 (Ando 1984) were used at the University of Leicester. Lower limits of detection (LLD) for XRF analyses were determined for the analytical method as a whole, incorporating all stages of sample preparation, including crushing, grinding, fusion, and pellet preparation. The standard deviation of replicate measurements was used to estimate LLDs as 3σ of the measured concentrations. Rhyolite Detection limits (reported in Table 1) are well below the average rhyolite compositions for most measured elements.

Results

Whole-rock chemistry

The four occurrences of HSRs studied here contain 75 − 77 wt% SiO_2 on an anhydrous basis (Table 1). They are subalkaline with 6 − 9 wt% $Na_2O + K_2O$ (Table 1), and 11 − 13 wt% Al_2O_3 (Fig. 2). There is no systematic pattern of major element enrichment (e.g., K_2O) or depletion (e.g., CaO) to accompany the increase in SiO_2 when compared to CV rhyolites (Fig. 2), e.g., from Torfajokull (McGarvie et al. 1990) or Kerlingarfjoll (Flude et al. 2010).

Trace element concentrations (Fig. 3) range between 50 − 100 ppm Sr, 50–100 ppm Rb, and 100 − 120 ppm Y, and are comparable with rhyolites from CVs (40–80 ppm, 50–100 ppm and 100–150 ppm respectively). Contrastingly, Nb is higher in rhyolites from CVs (140 − 160 ppm) than in HSRs (50–70 ppm). Zr and Ba have a wider range of concentrations in HSRs (200 − 450 ppm and 500 − 650 ppm respectively) than in rhyolites associated with CVs (Zr 500–900 ppm; Ba 200 − 800 ppm). This is a defining characteristic of the isolated HSR: their incompatible trace element concentrations are substantially lower than their CV counterparts (e.g., from Torfajökull; Fig. 4).

Petrography and mineral chemistry

Samples from all four HSR occurrences are mostly glassy (Fig. 5a-d) showing in some of the thin sections the development of microlites of pyroxene or plagioclase, with a trachytic/hyalopilitic texture. Ketilhyrnur sample contains only four small (~ 0.3mm) hedenbergite phenocrysts (Mg# ~ 5; Table 2), and Prestahnúkur samples contain up to 6% phenocrysts by volume of (in decreasing abundance) plagioclase, quartz, olivine, clinopyroxene, ilmenite and allanite. Plagioclase (< 5 vol%) occurs as microlites and phenocrysts. The phenocrysts are tabular and 0.3–0.8 mm in length, and occur as single crystals, or in glomerocrysts together with olivine and/or clinopyroxene. Plagioclase crystals are largely euhedral to subhedral, but with many examples of fragmented crystals, often distributed in bands. Plagioclase compositions vary between An_{24} and $An_{30,}$ i.e., oligoclase up to the boundary with andesine. Microprobe analyses of plagioclase phenocrysts are presented in Table 3 and in the Supplementary Material. Quartz (1 − 3 vol%) is typically euhedral, equant and 0.3 − 0.4 mm in length, often showing embayments. Olivine is almost pure fayalite ($\%Fo_{1-2}$), 0.1 − 0.3 mm long, and occurs as fragmented or resorbed equant subhedral crystals either as single occurrences or as glomerocrystic clusters (Fig. 5a), with either

Table 1 Whole rock geochemistry of major (wt%) and trace elements (ppm) of non-CV Icelandic High Silica Rhyolites. Column LLD indicates the lower detection limits for the analyses, see text for more details

		Prestahnúkur						Sultarfell		Maelifell		Ketilhyrnur	
	LLD	PK1	PK2	PK3	PK4	PK6	PK7	JM-5	JM-76	MAEL1	MAEL4	KET00/151	KET00/161
SiO_2	0.01	77.14	76.80	77.12	77.04	76.85	76.61	75.55	75.22	76.52	74.75	74.98	75.22
TiO_2	0.001	0.12	0.12	0.12	0.12	0.13	0.12	0.13	0.12	0.17	0.19	0.18	0.19
Al_2O_3	0.008	12.05	12.17	12.19	12.19	12.16	12.11	13.10	12.98	11.81	11.63	12.32	12.41
Fe_2O_3	0.001	1.59	1.74	1.74	1.73	1.75	1.73	1.48	1.59	2.62	2.68	2.75	2.75
MnO	0.001	0.04	0.05	0.05	0.05	0.05	0.05	0.05	0.05	0.06	0.06	0.08	0.08
MgO	0.008	0.03	0.03	0.01	0.02	0.02	0.02	0.04	0.05	0.03	0.07	0.01	0.01
CaO	0.001	0.96	1.05	1.04	1.04	1.05	1.04	0.81	0.77	1.47	1.46	1.35	1.35
Na_2O	0.02	4.29	4.39	4.37	4.41	4.42	4.40	4.42	4.29	4.54	4.43	4.61	4.59
K_2O	0.002	3.41	3.29	3.33	3.28	3.28	3.30	4.02	4.14	2.42	2.35	3.04	3.06
P_2O_5	0.002	0.01	0.01	0.01	0.01	0.01	0.01	0.01	0.01	0.02	0.02	0.02	0.02
LOI	0.01	0.37	0.32	0.33	0.24	0.36	0.36	0.31	0.22	0.41	2.94	0.16	0.19
Total		100.00	99.97	100.31	100.12	100.08	99.76	99.92	99.45	100.06	100.58	99.50	99.87
Rb	5	82	79	79	79	80	79	98	104	58	56	75	76
Sr	5	68	78	76	76	78	77	60	55	85	84	80	81
Y	6	98	110	110	109	110	110	54	55	134	132	104	105
Zr	10	201	259	248	249	256	254	226	216	405	397	411	413
Nb	15	59	68	66	65	66	66	52	54	51	49	63	63
Ba	15	623	619	629	620	627	628	619	613	518	524	572	550
Pb	15	8	8	9	6	8	6	8	8	5	5	6	5
Th	10	12	12	13	14	14	13	13	13	7	7	9	8
U	10	2	3	4	4	4	4	3	4	2	2	2	2
Zn	3	97	117	115	116	119	116	55	53	144	140	126	124
Ga	5	21	21	23	21	22	22	19	19	22	23	22	21

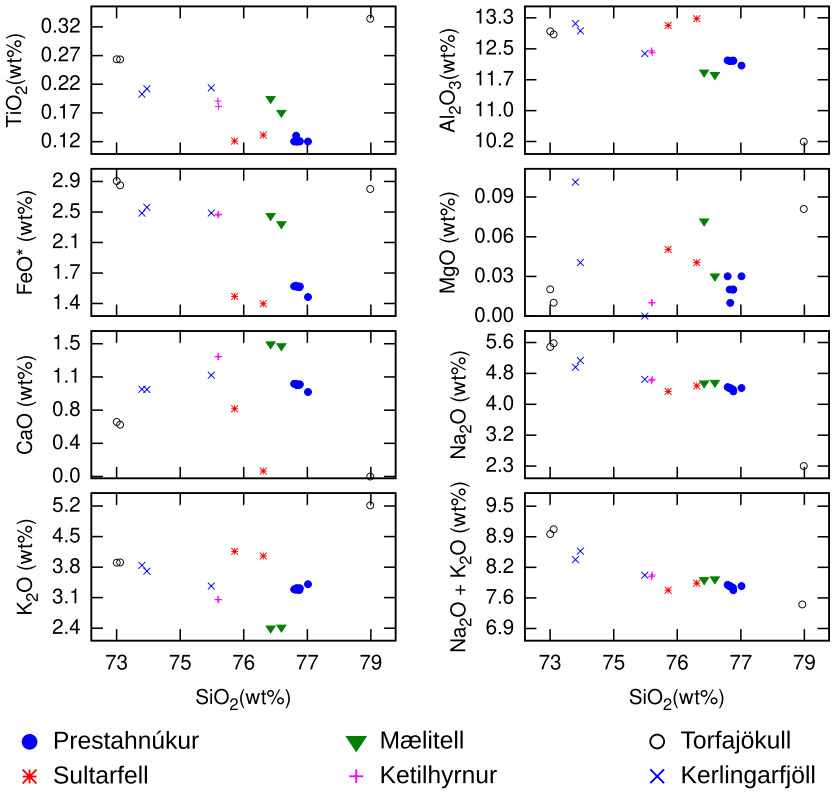

Fig. 2 Major element variation diagrams versus SiO_2 (wt%) of Prestahnúkur (filled blue circles), Sultarfell (red asterisks), Maelifell (green triangles) and Ketilhyrnur (pink crosses). Analyses from Torfajökull (open black circles; McGarvie et al. 1990), a southern flank zone rhyolite, and Kerlingarfjoll (blue crosses; Flude et al. 2010), a rift zone rhyolite are given for comparison

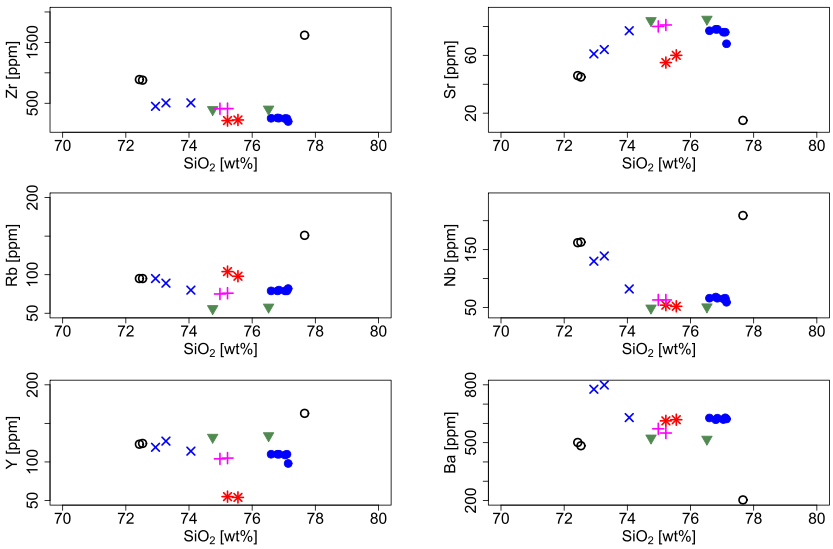

Fig. 3 Trace element (ppm) variation diagrams versus SiO_2 (wt%). Same symbols and samples from Fig. 2

plagioclase or clinopyroxene (1–2 vol%). Microprobe analyses are presented in Table 4, and in the Supplementary Material. Clinopyroxene (1–2 vol%) is typically hedenbergite with a Mg# of ~ 2–5%, found as prismatic euhedral and fragmented individual crystals or with plagioclase or olivine (Fig. 5a). Analyses of clinopyroxene are reported in Table 2.

A few examples of euhedral oxides (Fig. 5d) occur (Table 5). Recalculated analyses as magnetite, using 32 oxygens in the formula do not produce an adequate stoichiometry, but using three oxygens in the formula yields a stoichiometry closer to ilmenite, consistent with the clinopyroxene mineral chemistry (i.e., all iron recalculated as ferrous iron).

Allanite occurs as rare euhedral but fragmented ~ 0.3 mm long crystals in only one of the thin sections (Fig. 5b, c), with microprobe analyses presented in Table 6. Although the totals are close to ~ 97 wt%, the recalculated

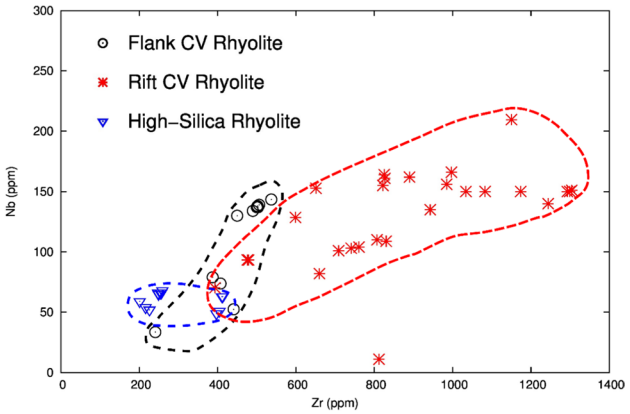

Fig. 4 Zr (ppm) vs Nb (ppm) variation diagram for the HSR (blue open triangles), compared with rhyolites and HSRs derived from flank CVs (black open circles) and rift CVs (red stars). Data (McGarvie, unpublished) from Krafla, Fremri Namur, Hagöngur and Kerlingarfjöll (flank CV); Snæfellsjökull, Ljósufjöll, Hekla, Torfajökull, Katla, Öræfajökull, Snæfell and Tindfjallajökull (rift CV)

analyses as cation per formula unit based on 12.5 oxygens produces a stoichiometry close to the ideal allanite formula (i.e., ~8 cations).

Groundmass glass was analysed in samples from Mælifell, Ketilhyrnur and Prestahnúkur (Table 7 & Supplementary Material). SiO_2 content varies between ~78 and ~80 wt% in all the samples. Variation in all the other major elements is, in general, less than 1 wt%, with Mælifell groundmass comparatively richer in total iron and poorer in K_2O and Al_2O_3 than those from Ketilhyrnur and Prestahnúkur. McGarvie et al. (2007) noted that Prestahnúkur has the highest SiO_2 content of any unaltered Icelandic rhyolite, with an average glass composition of 78.3 wt% SiO_2.

Modelling approach and constraints

Based solely on the chemical and mineral composition of the studied HSRs, it is not straightforward to determine whether fractional crystallisation, partial melting, or a combination of both are the mechanisms involved in their petrogenesis. Regardless of the specific mechanism, the alkali feldspar-silica cotectic in the haplogranite system (Blundy and Cashmann 2001) constrains the depth at which HSRs evolve in the crust. For example, at Krafla, HSR melts are found at ~2.1 km equating a lithostatic pressure of ~70 MPa, assuming a crustal density of 2700 kg m^3, typical of Icelandic basalts. This is consistent with a range of shallow depths, determined by Gualda and Ghiorso (2013) to be between 1.8 and 3.6 km, equivalent to 50 to 200 MPa lithostatic pressures, assuming the same crustal density. Based on these constraints, we explore first to what extent a one-step extreme fractional crystallisation mechanism, starting from a basaltic composition at shallow depths (i.e., pressures less than 100 MPa) or during polybaric decompression can produce HSRs. We also explore the conditions in which partial melting of Icelandic crustal lithologies could take place, and if that is the case, what is the likely source composition. As the Icelandic crust (IC) is thought to represent a thicker version of the normal oceanic crust, reaching up to 40 km in thickness (Foulger et al. 2003), potential crustal shallow sources are thick basaltic lava layers, dykes, and sills (Friðleifsson et al. 2014), while the lower IC would contain gabbro layers, often inferred to also include pockets of plagiogranite/tonalite (Sigurdsson 1977; Foulger et al. 2003).

As the partial melting of a basaltic/gabbroic crust is highly unlikely due to their high-temperature solidus (around 1000 °C at a pressure of 100 MPa; Lambert and Wyllie 1972), we examine here the more likely partial melting of plagiogranites, formed during the crystallisation of basaltic melts, which punctuates (albeit in very small volumes) the oceanic crust (Coleman and Peterman 1975; Coleman and Donato 1979), and have been recently found in the Icelandic crust (Zierenberg et al. 2017; Friðleifsson et al. 2020). Plagiogranites have lower melting points (between 650 and 850 °C, at ~100 MPa pressure) and are well known to have low concentrations of incompatible elements, as they are derived from a depleted mantle source (e.g., Coleman and Peterman 1975; Coleman and Donato 1979; Gerlach et al. 1981; Floyd et al. 1998; Foulger and Anderson 2005; Rollinson 2009). For example, a typical plagiogranite contains ~100 ppm Zr (e.g., Coleman and Donato 1979), which, during partial melting, may enrich in comparable amounts in the HSRs reported here.

Partial melting of plagiogranites was previously proposed as a possible petrogenetic mechanism for the generation of all Icelandic rhyolites (Sigurdsson 1977), the mechanism relying on large amounts of plagiogranites occurring in the IC. In the average oceanic crust, plagiogranites are scarce, rarely exceeding 1 vol% of its total volume (Floyd et al. 1998; Gamal El Dien et al. 2021), which should be also the case in the IC, if it is just a thicker version of normal oceanic crust.

alphaMELTS calculations

To account for the range of starting basaltic compositions in Iceland, representative depleted, enriched, and a transitional basalt (Tables 8 and 9), have been selected from the GEOROC pre-compiled Icelandic database (Lehnert et al. 2000) using the k-medoids algorithm (Jin and Han 2011). We also consider in the models the low concentrations of the incompatible elements Zr and Nb (Fig. 4), as their concentrations in HSR are comparable with those in the average enriched Icelandic basalt (e.g., Lehnert et al. 2000).

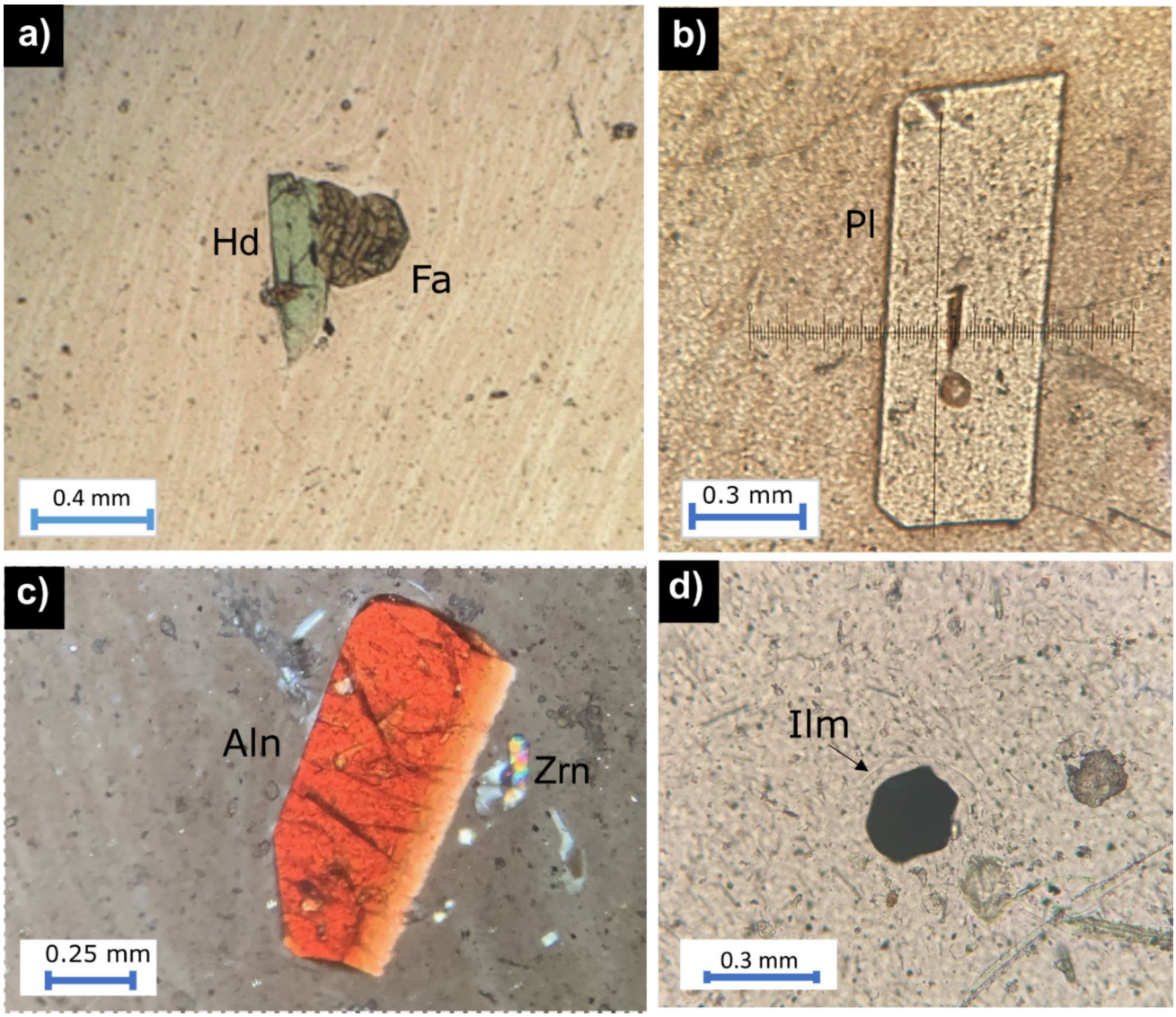

Fig. 5 Photomicrographs from Prestahnúkur sample PK1. a) Glomerocryst of fayalitic olivine and fragmented hedenbergite in a glassy banded matrix (PPL) b) Euhedral crystal of plagioclase featuring an elongated melt inclusion (PPL) c) Subhedral crystal of allanite and euhedral zircon in a glassy groundmass (XPL) d) Euhedral (trigonal) ilmenite in a glassy groundmass (PPL). Mineral abbreviations following Whitney and Evans (2010)

To test the models, we used alphaMELTS (Smith and Asimow 2005), a command line front-end of rhyolite-MELTS 1.0.2 (Ghiorso and Sack 1995; Asimow and Ghiorso 1998; Gualda et al. 2012), for the evolution of major and trace elements and the expected mineralogy. To better constrain intrinsic conditions, normative mineralogy was calculated based upon the major element geochemistry of each HSR occurrence and plotted into the haplogranite system (Qz-Ab-Or) to estimate the pressure at which HSR melts were crystallising and evolving (Fig. 6).

The selected basalt analyses, representative of the three main types erupted in Iceland, were used as starting compositions to generate HSRs in a single fractional crystallisation process. The same analyses were then used in a two-step process, to first generate plagiogranites by fractional crystallisation, and then HSR by their partial melting. Runs were executed at 50, 100, and 300 MPa pressures, with a fixed oxygen fugacity of QFM-1 as previously proposed for Icelandic magmas (e.g., Charreteur et al. 2013) and runs with variable oxygen fugacities of QFM-1, QFM and QFM + 1 were executed with a fixed pressure of 100 MPa. Initial concentrations of ~ 1 wt% of water were added to the basaltic starting compositions as a reasonable estimation for an Icelandic basalt, and the speciation of the iron in the analyses was computed using rhyolite-MELTS using the oxygen fugacity buffer value

Table 2 Microprobe analyses of clinopyroxene in samples from Prestahnúkur and Ketilhyrnur, in wt%. Numbers of cations (apfu) based on 6O. Speciation of the iron calculated following Papike et al. (1974). fO_2 (expressed in QFM units), estimated following Cortés et al. (2006). Column LLD indicates lower detection limits of the analyses, see text for more details

	LLD	PK-1/1	PK-1/1	PK-4/1	PK-4/1	PK-6/1	PK-6/1	PK-6/1	KET0015	KET0015	KET0015	KET0015
SiO_2	0.03	47.58	47.89	47.36	47.24	47.71	47.71	47.47	46.89	47.39	47.32	47.06
TiO_2	0.03	0.24	0.21	0.24	0.27	0.23	0.22	0.22	0.57	0.45	0.55	0.57
Al_2O_3	0.03	0.52	0.47	0.55	0.56	0.57	0.53	0.52	1.90	1.04	1.55	1.66
FeO	0.03	31.00	29.36	30.50	31.43	30.56	30.31	30.37	29.03	29.56	29.73	29.83
MnO	0.024	0.97	0.94	0.92	0.95	0.96	0.95	0.95	1.00	1.12	1.06	1.07
MgO	0.05	0.62	1.58	0.76	0.19	1.00	1.14	0.72	1.17	1.47	1.26	1.21
CaO	0.03	19.44	19.59	19.12	19.30	19.53	19.57	19.62	18.98	18.05	18.43	18.38
Na_2O	0.02	0.23	0.22	0.22	0.23	0.22	0.23	0.21	0.34	0.24	0.32	0.33
Cr_2O_3	0.04	0.00	0.01	0.00	0.00	0.00	0.00	0.00	0.10	0.19	0.17	0.13
Total		100.59	100.25	99.68	100.17	100.78	100.65	100.09	99.98	99.51	100.38	100.23
Si		1.967	1.970	1.971	1.966	1.964	1.964	1.968	1.933	1.965	1.946	1.940
Ti		0.007	0.007	0.008	0.008	0.007	0.007	0.007	0.018	0.014	0.017	0.018
Al		0.025	0.023	0.027	0.027	0.028	0.026	0.025	0.092	0.051	0.075	0.081
Fe^{3+}		0.045	0.041	0.034	0.042	0.048	0.050	0.041	0.033	0.011	0.024	0.031
Fe^{2+}		1.027	0.969	1.028	1.053	1.004	0.993	1.012	0.968	1.014	0.998	0.997
Mn		0.034	0.033	0.032	0.033	0.033	0.033	0.033	0.035	0.039	0.037	0.037
Mg		0.038	0.097	0.047	0.012	0.061	0.070	0.045	0.072	0.091	0.077	0.074
Ca		0.861	0.863	0.852	0.861	0.861	0.863	0.872	0.838	0.802	0.812	0.812
Na		0.018	0.018	0.018	0.019	0.018	0.018	0.017	0.027	0.019	0.026	0.026
Cr		0.000	0.000	0.000	0.000	0.000	0.000	0.000	0.000	0.000	0.000	0.000
Mg#		3.48	8.82	4.26	1.07	5.59	6.38	4.08	6.69	7.94	6.95	6.71
cation sum		4.02	4.02	4.02	4.02	4.02	4.03	4.02	4.02	4.01	4.01	4.02
oxygens		6	6	6	6	6	6	6	6	6	6	6
fO_2		–0.56	–0.58	–0.65	–0.60	–0.53	–0.50	–0.59	–0.65	–0.85	–0.73	–0.67

Table 3 Representative microprobe analyses of feldspars in samples from Prestahnúkur, in wt%. Numbers of cations (apfu) based on 8O. Column LLD indicates the lower detection limits of the analyses, see text for more details

	LLD	PK-1/1	PK-1/1	PK-1/1	PK-1/2	PK-1/2	PK-1/2	PK-4/2	PK-4/2	PK-4/2	PK-4/2	PK-4/2	PK-6/1	PK-6/1	PK-6/1	PK-6/1	PK-6/1
SiO_2	0.03	61.86	61.16	61.95	61.43	62.17	60.83	61.89	61.57	61.96	61.69	61.65	62.79	61.49	61.02	61.24	62.29
TiO_2	0.03	0.00	0.02	0.01	0.01	0.00	0.01	0.02	0.01	0.00	0.00	0.01	0.01	0.05	0.02	0.03	0.02
Al_2O_3	0.03	23.41	23.43	23.27	23.89	23.29	24.12	23.70	23.80	23.87	23.57	23.80	23.08	23.75	23.52	23.80	23.48
FeO	0.03	0.19	0.21	0.18	0.19	0.18	0.22	0.19	0.19	0.19	0.20	0.19	0.20	0.29	0.18	0.21	0.19
CaO	0.03	5.38	5.50	5.21	5.59	5.15	6.06	5.61	5.71	5.66	5.50	5.77	4.95	5.64	5.69	5.82	5.25
Na_2O	0.02	8.09	8.08	8.28	7.85	8.22	7.74	7.90	7.87	7.89	7.92	7.90	8.40	8.03	7.93	7.83	8.20
K_2O	0.05	0.49	0.47	0.49	0.47	0.52	0.39	0.43	0.40	0.42	0.42	0.42	0.50	0.44	0.44	0.42	0.44
BaO	0.09	0.04	0.05	0.06	0.06	0.07	0.06	0.03	0.06	0.05	0.01	0.04	0.02	0.07	0.03	0.03	0.05
Total		99.44	98.92	99.47	99.47	99.60	99.44	99.77	99.61	100.04	99.31	99.78	99.95	99.74	98.83	99.36	99.91
Si		2.762	2.749	2.766	2.743	2.771	2.722	2.753	2.745	2.749	2.756	2.745	2.785	2.742	2.744	2.739	2.766
Al		1.232	1.241	1.225	1.257	1.223	1.272	1.243	1.251	1.249	1.241	1.249	1.207	1.248	1.247	1.255	1.229
Ti		0.000	0.001	0.000	0.000	0.000	0.000	0.001	0.000	0.000	0.000	0.000	0.000	0.002	0.001	0.001	0.001
Fe		0.007	0.008	0.007	0.007	0.007	0.008	0.007	0.007	0.007	0.007	0.007	0.007	0.011	0.007	0.008	0.007
Ca		0.257	0.265	0.249	0.267	0.246	0.291	0.268	0.273	0.269	0.263	0.275	0.235	0.269	0.274	0.279	0.250
Na		0.700	0.704	0.717	0.680	0.710	0.671	0.681	0.681	0.679	0.686	0.682	0.722	0.694	0.691	0.679	0.706
K		0.028	0.027	0.028	0.027	0.030	0.022	0.024	0.023	0.024	0.024	0.024	0.029	0.025	0.025	0.024	0.025
Ba		0.001	0.001	0.001	0.001	0.001	0.001	0.001	0.001	0.001	0.000	0.001	0.000	0.001	0.001	0.000	0.001
cation sum		4.99	4.99	4.99	4.98	4.99	4.99	4.98	4.98	4.98	4.98	4.98	4.99	4.99	4.99	4.98	4.98
oxygens		8	8	8	8	8	8	8	8	8	8	8	8	8	8	8	8
Or		2.81	2.71	2.83	2.73	3.01	2.28	2.50	2.35	2.42	2.48	2.44	2.89	2.55	2.53	2.42	2.56
Ab		71.07	70.69	72.08	69.82	72.06	68.19	70.00	69.69	69.88	70.40	69.52	73.28	70.22	69.79	69.20	71.99
An		26.12	26.60	25.09	27.46	24.93	29.53	27.50	27.96	27.70	27.02	28.04	23.86	27.24	27.68	28.38	25.45

Table 4 Representative microprobe analyses of Olivine in samples from Prestahnúkur, in wt%. Numbers of cations (apfu) based on 4O. Column LLD indicates the lower detection limits of the analyses, see text for more details

	LLD	PK-1/1	PK-1/1	PK-1/2	PK-1/2	PK-1/2	PK-4/2	PK-4/2	PK-4/2	PK-6/1	PK-6/1
SiO_2	0.03	29.50	29.58	29.99	29.83	30.76	29.87	29.78	29.75	29.70	29.70
TiO_2	0.03	0.03	0.00	0.00	0.04	0.00	0.01	0.00	0.01	0.07	0.07
Al_2O_3	0.03	0.00	0.00	0.00	0.01	0.02	0.01	0.00	0.01	0.00	0.00
FeO	0.03	67.77	67.99	67.29	67.47	66.79	67.39	67.67	67.81	67.05	67.05
MnO	0.03	2.24	2.22	2.30	2.30	2.25	2.26	2.31	2.28	2.21	2.21
MgO	0.05	0.92	0.88	0.43	0.40	0.43	0.40	0.42	0.43	0.42	0.42
CaO	0.03	0.24	0.23	0.27	0.26	0.26	0.27	0.26	0.26	0.36	0.36
Na_2O	0.02	0.00	0.01	0.01	0.00	0.03	0.02	0.01	0.00	0.00	0.00
Cr_2O_3	0.04	0.00	0.00	0.01	0.01	0.00	0.01	0.00	0.01	0.00	0.00
Total		100.70	100.92	100.29	100.32	100.53	100.23	100.45	100.56	99.82	99.82
Si		0.990	0.990	1.007	1.002	1.023	1.005	1.001	0.999	1.003	1.003
Al		0.000	0.000	0.000	0.000	0.001	0.000	0.000	0.000	0.000	0.000
Ti		0.001	0.000	0.000	0.001	0.000	0.000	0.000	0.000	0.002	0.002
Fe^{2+}		1.901	1.904	1.889	1.897	1.858	1.895	1.902	1.905	1.893	1.893
Mn		0.064	0.063	0.065	0.066	0.063	0.064	0.066	0.065	0.063	0.063
Mg		0.046	0.044	0.021	0.020	0.021	0.020	0.021	0.022	0.021	0.021
Ca		0.009	0.008	0.000	0.000	0.000	0.000	0.000	0.000	0.013	0.013
Na		0.000	0.001	0.010	0.009	0.009	0.010	0.009	0.009	0.000	0.000
Cr		0.000	0.000	0.000	0.000	0.002	0.001	0.001	0.000	0.000	0.000
cation sum		3.010	3.010	2.994	2.996	2.978	2.996	2.999	3.001	2.995	2.995
oxygens		4	4	4	4	4	4	4	4	4	4
Fa %		97.65	97.73	98.89	98.96	98.87	98.95	98.92	98.88	98.89	98.89

Table 5 Microprobe Analyses of Ilmenite in samples from Prestahnúkur, in wt%. Numbers of cations (apfu) based on 3O. Column LLD indicates the lower detection limits of the analyses, see text for more details

	LLD	PK-1/1	PK-1/1	PK-1/1	PK-1/1	PK-6/1	PK-6/1
TiO_2	0.03	50.12	50.32	50.27	50.33	49.75	50.29
Al_2O_3	0.03	0.05	0.05	0.02	0.03	0.05	0.02
Cr_2O_3	0.04	0.00	0.00	0.00	0.01	0.00	0.01
FeO	0.03	47.88	48.00	48.10	48.13	47.59	48.08
MnO	0.03	1.15	1.13	1.11	1.18	1.12	1.13
MgO	0.05	0.09	0.07	0.08	0.08	0.03	0.03
Total		99.28	99.56	99.58	99.77	98.54	99.56
Ti		0.970	0.971	0.970	0.970	0.970	0.971
Al		0.002	0.002	0.001	0.001	0.002	0.001
Cr		0.000	0.000	0.000	0.000	0.000	0.000
Fe^{2+}		1.030	1.029	1.032	1.031	1.032	1.032
Mn		0.025	0.025	0.024	0.026	0.025	0.025
Mg		0.003	0.003	0.003	0.003	0.001	0.001
cation sum		2.03	2.03	2.03	2.03	2.03	2.03
oxygens		3	3	3	3	3	3

of each run at the liquidus temperature. Tables 8 and 9 summarises the starting compositions after the speciation of iron was calculated.

Testing a single step fractional crystallisation model reveals that after 80–91 vol% crystallisation (Fig. 7a and b), the three compositions follow similar liquid lines of descent with expected variations controlled by the pressure and to lesser extent, by differences in the starting compositions. At 100 MPa, the compositions reach ~73 wt% SiO_2 and does not increase further as the system reaches the cotectic or the system crosses the solidus (Fig. 7a and b). As expected, at lower pressures (50 MPa) the models reach higher SiO_2 values (~74–75 wt%) with one polybaric run crossing 75 wt% (Fig. 7a and b). At higher pressures (300 MPa), silica concentrations remain below 66 wt% (Fig. 7a and b). Our findings also suggest that changes in oxygen fugacity play a negligible role in the silica content with evolution (Fig. 7c and d). The

Table 6 Microprobe analysis of Allanite crystals in samples from Prestahnúkur, in wt%. Numbers of cations (apfu) based on 12.5O. Column LLD indicates the lower detection limits of the analyses, see text for more details. An estimation for REE lower detection limits is also given in the column based on Reed and Buckley (2018)

	LLD	PK-1/2	PK-1/2	PK-1/2	PK-1/2	PK-1/2	PK-1/2	PK-4/2	PK-4/2	PK-4/2	PK-4/2
SiO_2	0.03	30.63	30.77	31.08	30.79	30.40	30.35	30.30	30.24	30.17	30.64
TiO_2	0.03	2.58	2.64	2.63	2.52	2.87	2.77	2.65	2.70	2.65	2.61
Al_2O_3	0.03	12.17	12.06	12.09	11.98	11.61	11.88	12.00	11.98	11.88	12.15
Cr_2O_3	0.04	0.00	0.00	0.00	0.00	0.00	0.00	0.00	0.00	0.00	0.00
FeO	0.03	16.95	16.94	17.03	17.14	17.20	16.93	17.10	17.17	17.10	17.04
MnO	0.03	0.01	0.00	0.00	0.00	0.00	0.01	0.00	0.00	0.00	0.00
MgO	0.05	0.16	0.17	0.18	0.17	0.20	0.22	0.06	0.08	0.08	0.08
CaO	0.03	9.98	10.04	10.01	9.97	9.77	9.76	9.55	9.62	9.56	9.92
La_2O_3	0.008–0.02	6.03	6.11	6.22	6.34	6.68	6.75	7.31	7.28	7.25	6.82
Ce_2O_3	0.008–0.02	12.36	12.51	12.42	12.52	12.57	12.60	12.96	12.89	12.89	12.69
Pr_2O_3	0.008–0.02	1.15	1.15	1.16	1.16	1.09	1.06	1.14	1.06	1.12	1.13
Nd_2O_3	0.008–0.02	4.43	4.37	4.39	4.26	4.09	4.14	4.10	4.13	4.19	4.13
Gd_2O_3	0.008–0.03	0.16	0.12	0.13	0.09	0.11	0.14	0.08	0.03	0.05	0.10
Sm_2O_3	0.008–0.03	0.55	0.56	0.55	0.52	0.48	0.50	0.42	0.45	0.45	0.48
Total		97.18	97.43	97.87	97.45	97.06	97.11	97.66	97.64	97.38	97.79
Si		3.059	3.065	3.078	3.071	3.054	3.047	3.040	3.034	3.038	3.052
Ti		0.194	0.198	0.196	0.189	0.217	0.209	0.200	0.204	0.201	0.196
Al		1.432	1.416	1.411	1.408	1.375	1.405	1.419	1.417	1.410	1.426
Cr		0.000	0.000	0.000	0.000	0.000	0.000	0.000	0.000	0.000	0.000
Fe^{+2}		1.416	1.411	1.410	1.429	1.445	1.421	1.435	1.441	1.440	1.420
Mn		0.001	0.000	0.000	0.000	0.000	0.001	0.000	0.000	0.000	0.000
Mg		0.024	0.025	0.026	0.026	0.030	0.033	0.009	0.012	0.012	0.012
Ca		1.067	1.072	1.062	1.066	1.052	1.050	1.027	1.034	1.031	1.059
La		0.222	0.224	0.227	0.233	0.248	0.250	0.270	0.269	0.269	0.251
Ce		0.452	0.456	0.450	0.457	0.462	0.463	0.476	0.474	0.475	0.463
Pr		0.042	0.042	0.042	0.042	0.040	0.039	0.042	0.039	0.041	0.041
Nd		0.158	0.156	0.155	0.152	0.147	0.148	0.147	0.148	0.151	0.147
Gd		0.005	0.004	0.004	0.003	0.004	0.005	0.003	0.001	0.002	0.003
Sm		0.020	0.020	0.020	0.019	0.018	0.018	0.015	0.016	0.017	0.017
cation sum		8.09	8.09	8.08	8.10	8.09	8.09	8.08	8.09	8.09	8.09
oxygens		12.5	12.5	12.5	12.5	12.5	12.5	12.5	12.5	12.5	12.5

Table 7 Microprobe analyses of groundmass glass in HSRs. Column LLD indicates the lower detection limits of the analyses, see text for more details

		Mælifell		Prestahnúkur		Ketilhyrnur					
	LLD	MAEL-2	MAEL-2	PK-1/1	PK-1/2	PK-4/2	PK-4/2	KET0015	KET0015	KET0015	KET0015
SiO_2	0.03	78.39	78.07	78.11	79.39	78.90	79.26	77.84	78.82	79.95	79.07
TiO_2	0.03	0.17	0.17	0.09	0.09	0.09	0.09	0.17	0.18	0.16	0.18
Al_2O_3	0.03	11.89	11.92	12.14	12.27	12.24	12.34	12.67	12.77	12.55	12.83
FeO	0.03	2.40	2.43	1.22	1.19	1.25	1.10	2.28	1.47	0.98	1.06
MnO	0.03	0.05	0.07	0.03	0.03	0.04	0.05	0.07	0.07	0.07	0.06
MgO	0.05	0.01	0.02	0.00	0.00	0.00	0.00	0.01	0.01	0.01	0.01
CaO	0.03	1.42	1.40	0.84	0.86	0.86	0.89	1.22	1.15	1.05	1.26
Na_2O	0.02	1.14	1.23	2.06	1.29	1.19	1.10	0.67	0.63	0.61	0.59
K_2O	0.03	2.41	2.58	3.44	3.47	3.27	3.37	3.18	3.21	3.13	3.14
P_2O_5	0.05	0.02	0.02	0.00	0.01	0.00	0.01	0.01	0.01	0.01	0.02
ZnO	0.05	0.05	0.03	0.04	0.02	0.04	0.05	0.05	0.00	0.00	0.03
F	0.05	0.05	0.03	0.08	0.09	0.11	0.11	0.07	0.11	0.09	0.18
Cl	0.03	0.08	0.05	0.05	0.06	0.03	0.05	0.11	0.12	0.10	0.10
Total		98.08	98.00	98.11	98.75	98.01	98.43	98.33	98.56	98.71	98.54

Table 8 Summary of the data used for MELTS modelling and results of fractional crystallisation at 50 MPa and oxygen fugacity of QFM-1, and polybaric decompression (geothermal gradient dP/dT = 2.65 bar/ºC), starting with a pressure of 100 MPa. TºC is the liquidus temperature for the basalt and the temperature at which rhyolites are generated

Sample	Basalt 1864 (alkaline basalt)			Basalt 4590 (transitional alkaline basalt)			Basalt 2778 (Tholeiitic Basalt)		
	Start comp	50 MPa (wet)	Polybaric (wet)	Start comp	50 MPa (wet)	Polybaric (wet)	Start comp	50 MPa (wet)	Polybaric (wet)
		80% fx	81% fx		85% fx	85% fx		91% fx	92% fx
SiO_2	49.31	72.16	73.20	49.05	70.67	71.00	48.51	67.21	68.05
TiO_2	2.27	0.36	0.27	1.38	0.48	0.39	0.68	0.65	0.58
Al_2O_3	13.87	6.89	6.80	14.74	7.38	7.65	14.72	7.71	7.76
Fe_2O_3	5.74	0.22	0.22	0.54	0.08	0.08	0.43	0.17	0.14
FeO	8.64	4.99	3.80	10.89	6.17	5.18	8.82	8.97	7.93
MnO	0.23	0.33	0.34	0.20	0.37	0.38	0.17	0.45	0.47
MgO	5.35	0.01	0.01	7.53	0.01	0.02	11.38	0.02	0.02
CaO	10.69	4.72	4.16	12.11	5.76	5.23	12.90	6.66	6.34
Na_2O	2.76	5.73	5.79	2.05	4.94	5.01	1.62	4.92	5.01
K_2O	0.30	1.26	1.35	0.15	0.85	0.91	0.05	0.47	0.52
P_2O_5	0.31	0.62	0.64	0.14	0.64	0.64	0.05	0.56	0.63
H_2O	1.31	2.70	3.42	0.78	2.64	3.27	0.61	2.23	2.54
Total	100.78	99.99	100.00	99.56	99.99	99.76	99.94	100.02	99.99
TºC	1113	876	843	1169	894	873	1265	931	918
La	22	90	94	5.34	28	29	1.63	14	15
Rb	12	57	60	2.6	16	17	1.3	14	15
Sr	250	203	199	138	115	116	87.1	89	91
Y	29	107	111	26	116	117	16	110	111
Zr	137	626	659	70.2	420	435	30.8	310	328
Nb	15	70	74	8.1	50	52	1.7	18	19
Ba	124	454	475	47.3	218	225	17	124	130

results confirm that a fractional crystallisation model is almost able to generate HSR melts at lower pressures/depths (50 MPa), consistent with those found in CVs with a long-established magmatic system (e.g., Krafla), and it is also adequate to generate plagiogranites at relatively higher depths (> 100 MPa; Fig. 8).

At higher pressures, i.e., > 100 MPa, the expected crystallising phases are clinopyroxene, spinel and plagioclase. Calculating the normative mineralogy of these evolving melts and plotting these in a QAP diagram (Fig. 8) show that the residual melt reaches tonalitic (i.e., plagiogranite) compositions after 80–92 wt% of fractional crystallisation (Table 9). The process leaves an evolved melt (62–72 wt% SiO_2), enriched in incompatible elements, i.e.: ~ 300–600 ppm Zr, ~ 100–200 ppm Sr, 120–450 ppm Ba, 20–70 ppm Nb, 80–110 ppm Y, and ~ 10–60 ppm Rb (Table 9).

Partial melting of the plagiogranites was calculated using an equilibrium crystallisation model, assuming that the weight fraction of melt produced F is equal to 1-F from the equilibrium crystallisation model. Although reverse crystallisation overestimates melt fractions near the solidus, it is a reasonable estimation for moderate and high melt fractions (Ghiorso and Stolper 1999). Plagiogranite compositions were calculated from the compositions derived from the basalt fractionation models at evolved stages (Table 8).

In all cases, partial melting between 11 and 40 vol% of the generated plagiogranite, with temperatures between 500–750 ºC reproduces HSR most of the major element compositions (Table 9) comparable with the studied samples compositions (Table 1, Figs. 2 and 3), with up to 82 wt% SiO_2 in a recalculated dry analysis, however there are important discrepancies in CaO (3.5 −4.7 wt% in the model vs 0.8–1.4 wt% in the studied samples), Na_2O (4 −12 wt% in the model vs 0.6–2 wt% in the studied samples), and K_2O (0.2–1.3 wt% in the model vs 2.1–3.5 wt% in the studied samples).

Plagiogranites formed from both depleted and transitional basalts are also able to replicate (Fig. 9) most of the trace element geochemistry (i.e., ~ 50–115 ppm Y, ~ 340–760 ppm Ba and ~ 30–130 ppm Rb). However, all partial melting models over-estimate the concentrations of Zr, Nb and Sr. Compared with the single fractionation models (at 50 MPa constant pressure and polybaric decompression), although all of them can recreate well the trace elements concentrations, only the

Table 9 Summary of the data used for MELTS modelling and results of the two-step process based on 100 MPa and intrinsic oxygen fugacity of QFM-1. T°C is the liquidus temperature for the basalt and plagiogranite (plgr), and the temperature at which partial melting produces the HSRs

Sample	Basalt 1864	plgr 1	HSR1 (wet)	HSR1 (dry)	Basalt 4590	plgr 2	HSR2 (wet)	HSR2 (dry)	Basalt 2778	plgr 3	HSR3 (wet)	HSR3 (dry)
	Start comp	80% fx	15% pm		Start comp	92% fx	11% pm		Start comp	80% fx	40% pm	
SiO_2	49.31	72.16	71.9	75.45	49.05	66.36	72.39	77.04	48.51	62.5	78.73	82.01
TiO_2	2.27	0.36	0	0.00	1.38	0.66	0.03	0.03	0.68	0.67	0.16	0.17
Al_2O_3	13.87	6.89	0.32	0.34	14.74	8.02	1.7	1.81	14.72	11.18	5.67	5.91
Fe_2O_3	5.74	0.22	0.00	0.00	0.54	0.17	0.01	0.01	0.43	0.09	0.01	0.01
FeO	8.64	4.99	0.04	0.04	10.89	9.32	0.55	0.59	8.82	9.05	1.41	1.47
MnO	0.23	0.33	1.85	1.94	0.20	0.48	3.73	3.97	0.17	0.42	0.37	0.39
MgO	5.35	0.01	0.00	0.00	7.53	0.02	0.00	0.00	11.38	0.29	0.01	0.01
CaO	10.69	4.72	4.49	4.71	12.11	6.6	4.27	4.54	12.90	6.39	3.55	3.70
Na_2O	2.76	5.73	12.95	13.59	2.05	4.94	7.82	8.32	1.62	4.58	3.98	4.15
K_2O	0.30	1.27	0.27	0.28	0.15	0.49	0.77	0.82	0.05	0.63	1.26	1.31
P_2O_5	0.31	0.62	3.47	3.64	0.14	0.59	2.69	2.86	0.05	0.64	0.85	0.89
H_2O	1.31	2.7	4.69		0.78	2.35	6.04		0.61	3.55	3.99	
Total	100.78	100.00	99.98		99.56	100.00	100.00		99.94	99.99	99.99	
T°C	1113	876	500		1169	937	630		1265	938	750	
La	22	90	135		5.34	15	51		1.63	21	43	
Rb	12	57	312		2.6	15	134		1.3	12	29	
Sr	250	203	376		138	87	93		87.1	132	113	
Y	29	107	13		26	113	53		16	83	115	
Zr	137	626	3138		70.2	325	2255		30.8	300	698	
Nb	15	70	378		8.1	19	157		1.7	36	86	
Ba	124	454	2093		47.3	129	761		17	166	342	

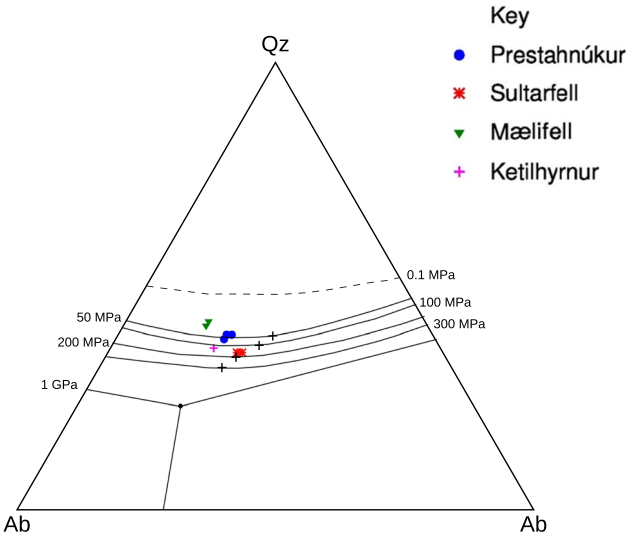

Fig. 6 Haplogranite ternary system with the location of the minima (black crosses) at different pressures (Gualda and Ghiorso 2013) and the calculated normative mineralogy from samples from Prestahnúkur, Sultarfell, Maelifell and Ketilhyrnur. After Tuttle and Bowen, (1958) and Blundy and Cashmann (2001). Symbols as in Fig. 2. (Mineral abbreviations following Whitney DL, Evans BW 2010)

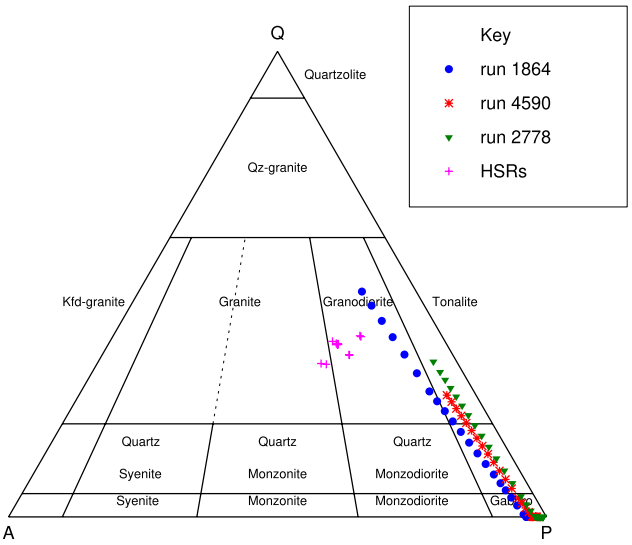

Fig. 8 QAP classification diagram (Le Maitre et al. 2002) showing the evolution of normative mineralogy from melts derived from fractional crystallisation models ran at 100 MPa and fO_2 = QFM-1. Normative HSR from the studied samples (pink crosses) are given for reference. Same starting compositions reported in Table 9

enriched basalt polybaric decompression run reaches a HSR silica content. The run still overestimates Zr, with a predicted concentration up to 300 ppm higher than the concentration measured in the studied samples (Table 1).

Mineralogy in Prestahnúkur samples

To test equilibrium between the HSR melt and the occurring mineralogy, a further crystallisation run in the HSR melt was calculated using rhyolite-MELTS in an equilibrium crystallisation run on the whole-rock major element composition of a Prestahnúkur sample (PK1). The crystallisation conditions were assumed to be the same (100 MPa and oxygen buffer QFM-1) as those used in the partial melting models. The calculation successfully reproduces some of the mineralogy found in Prestahnúkur samples. Fayalite, ilmenite, and hedenbergite are predicted by rhyolite-MELTS after the crystallisation of 20–25 vol% quartz and 35–36 vol% albite.

Plagioclase crystals are the most abundant mineral in the Prestahnúkur samples, and this is consistent with what is predicted by rhyolite-MELTS. However, the composition of these ranges from oligoclase to andesine (An_{25-30}), substantially more calcic than the compositions predicted by rhyolite-MELTS (up to ~An_{10}).

Allanite is a calcium-cerium-lanthanum-aluminium-iron sorosilicate that mainly occurs as accessory constituent in metamorphic or in granitic (Tindle 2008) to intermediate igneous rocks (e.g., in tonalites; Oziegbe et al. 2020), but it is extremely rare in effusive evolved volcanic rocks (e.g.,

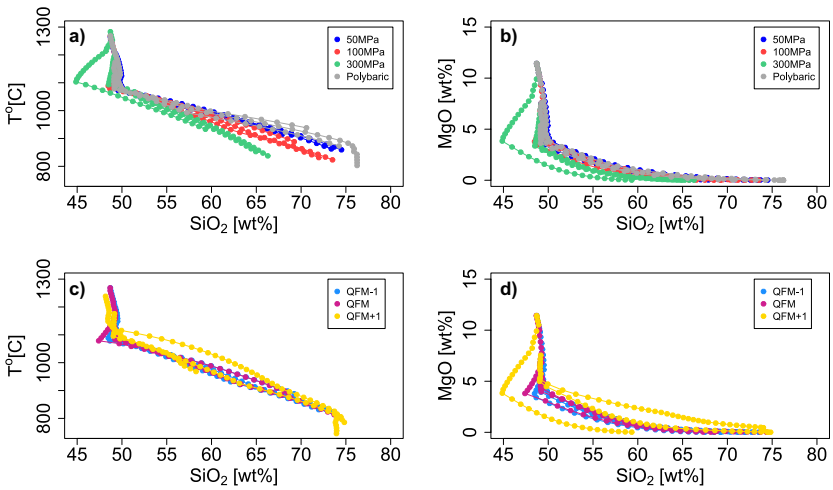

Fig. 7 **a**) Temperature (°C) vs SiO_2 (wt%) and **b**) MgO (wt%) vs SiO_2 (wt%) of rhyolite-MELTS runs starting from samples reported in Table 8. All these runs were calculated with oxygen fugacity of QFM-1. Pressure set at 50 MPa (blue lines), 100 MPa (red lines), 300 MPa (green lines) and polybaric fractionation with a gradient $\Delta T/\Delta P = 10$ °C/MPa. **c**) T(.°C) vs SiO_2 (wt%) and **d**) MgO (wt%) vs SiO_2 (wt%) of rhyolite-MELTS runs starting from the same gabbros. All these runs were calculated using a pressure of 100 MPa with oxygen fugacity of QFM-1 (blue lines), QFM (magenta lines) and QFM + 1 (amber lines)

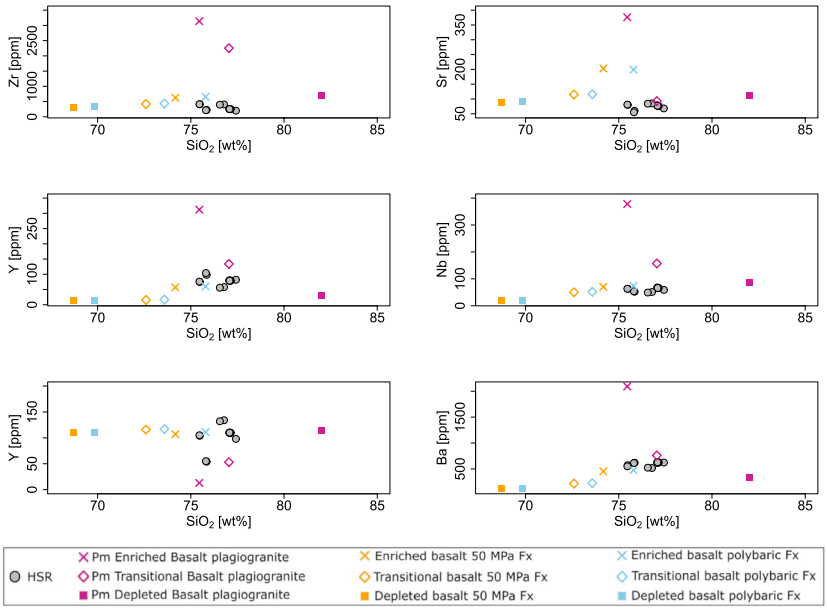

Fig. 9 Trace elements vs SiO_2 of alpha-MELTS runs reported in Table 8a and b; grey circles represent the HSR samples (Table 1). Pink symbols represent the HSR's generated by the partial melting (Pm) of plagiogranites formed by enriched basalts (crosses), transitional basalts (diamonds) and depleted basalts (squares). Orange symbols show the HSR's generated by fractional crystallisation (Fx) at 50 MPa of enriched basalts (crosses), transitional basalts (diamonds) and depleted basalts (squares). Blue symbols show HSR's generated from polybaric fractional crystallisation (Fx) of enriched basalts (crosses), transitional basalts (diamonds) and depleted basalts (squares)

Duggan 1976). In Iceland, it has been reported in pyroclastic rocks from the Reyðarfjörður drill hole (Schmincke and Viereck 1982) and in granodiorites and tonalites (Gurenko et al. 2015) but not in effusive rhyolites.

Fayalite crystals, using the FeO/MgO distribution coefficient with the equilibrium melt assuming the speciation of iron of the glass based on the QFM-1 oxygen fugacity buffer (calculated using Cortés et al. 2006), are likely to be in equilibrium with their surrounding glass, assuming a K_D value of 0.32. Following Putirka (2008), melt in equilibrium with the composition of the olivine crystals occurring in the samples (Table 3) should have MgO ~ 0.01 wt%, a concentration consistent with the concentration found in the glass analyses (Table 7), and in the whole-rock analyses (Table 1). Caution is necessary here, as it is unknown whether the Roeder and Emslie (1970) criterion holds true for fayalitic olivine.

Discussion

In summary, HSRs major element compositions reported in this work can in theory be generated by extreme fractional crystallisation under a polybaric decompression at shallow crustal levels starting from an enriched basalt, or by the partial melting of evolved compositions previously crystalised and perched in the IC. However, the additional constrains given by the inconsistencies in trace elements concentrations, specifically Zr, favour a partial melting model. Although some studies have proposed zircon fractionation to explain trace and REE elements patterns in volcanic rocks (e.g., Evans and Hanson 1993), such fractionation is problematic in evolved melts due to their high viscosities. But critically, zircon crystallisation fixes Zr in the solid phase. As the melting point of zircon crystals at atmospheric pressure is ~ 1676 °C in the ZrO_2-SiO_2 system (Butterman and Foster 1967), the partial melting of any hosting rock will leave most of the zircon in the restite; up to ~ 90% of the crystals after a crustal melting event at a temperature of 750 °C (Yakymchuk and Brown 2014).

Therefore, if this mineral phase crystallises in plagiogranites (a common accesory mineral in intrusive rocks; Deer et al. 2013), their subsequent partial melting will likely generate melts that are depleted in Zr, perhaps ocasionally incorporating few xenocrystic zircons in the volcanic products, as found in the Prestahnúkur samples. Depletion in Nb can be equally atributed to an analogue effect, due to the refractory nature of the pair Ilmenite-Magnetite (Buddington and Lindsley 1964), which crucially crystallise in evolved compositions and comparatively higher pressures. The difference in Sr concentration between the model and the studied samples (Fig. 9) is consistent with the discrepancies in CaO and alkalis content between models and the studied samples, perhaps suggesting fractionation of plagioclase prior melt ascent, not considered in the models.

Additionally, as the depleted mantle and the IC are mainly dry, a single-step process cannot generate melts with a reasonable volatile content consistent with the volatile content in the four HSR occurrences as they are effusive lavas, likely with relevant Cl and F concentrations as found in the glass analyses from Prestahnúkur (McGarvie et al. 2007). Similarly, the deuterium and oxygen isotope

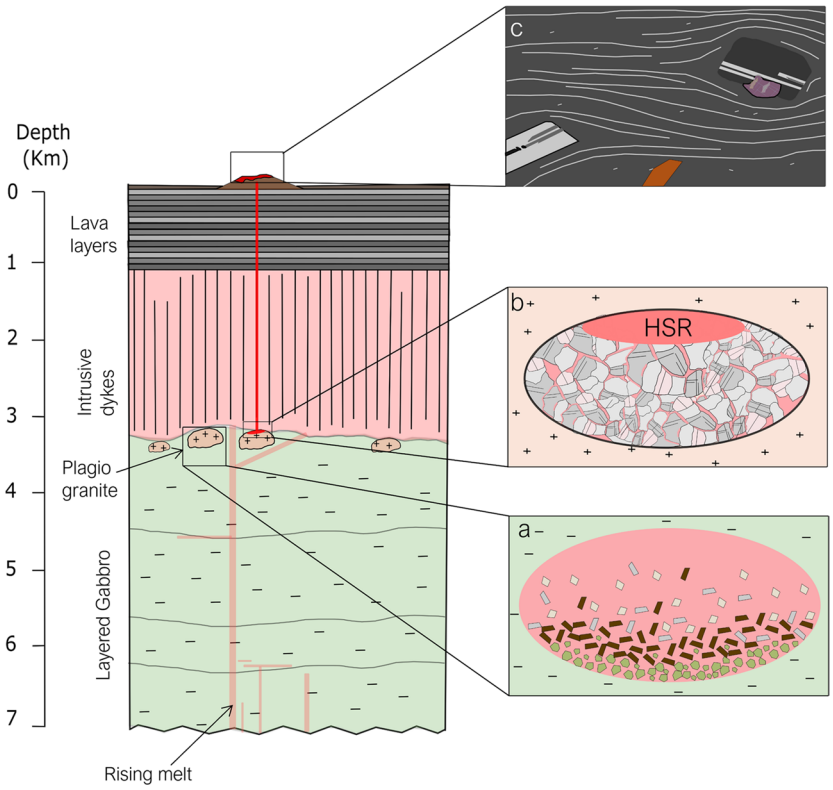

Fig. 10 Petrogenetic model for Icelandic HSR. Diagram displays only the top 7 km of the Icelandic crust (IC). (**a**) Fractional crystallisation starting from a basaltic melt. This produces plagiogranites, with the predominant crystallisation of plagioclases and pyroxene, and likely zircon and allanite. (**b**) Intruding/rising melts from either the rift or mantle plume trigger the partial melting of the plagiogranite generating HSR melts rising through the IC. (c) Deposits of high silica rhyolite display vitric textures with few phenocrysts, typically plagioclase, and xenocrysts of allanite and zircon

signatures of magmatic water within Krafla IDDP-1 indicate an important contribution from hydrothermal fluids in the petrogenesis of its HSR (Saubin et al. 2021), consistent with its origin from within a long-lived, caldera-hosted hydrothermal system. Under the absence of a hydrothermal system in the isolated examples, an obvious process to concentrate volatiles could be by first generating evolved rocks by fractional crystallisation and then generate HSRs by their partial melting.

Assuming that HSRs form by 10–20 vol% partial melting of a plagiogranite source, the partial melting model requires a minimum of 30–60 km^3 of plagiogranite in the Icelandic crust, and specifically 8–16 km^3 of plagiogranite to generate Prestahnukur's HSRs. As stated earlier, plagiogranite has been hypothesised to occur as pockets in the Icelandic crust (Sigurdsson 1977; Foulger et al. 2003) and it has been found in the Icelandic crust in the IDDP-2 core samples (e.g., Zierenberg et al. 2017; Friðleifsson et al. 2020). Given the small volumes of the four non-central-volcano HSR occurrences in Iceland, a model involving partial melting of plagiogranite is plausible.

Based on the overall crystal textures of the minor occurrences found in Prestahnukur samples (e.g., fragmented crystals of allanite or quartz with embayments), suggest that some of the mineralogy might be xenocrystic, dragged and transported by the forming melt from a mush zone, or remobilised from silicic intrusions (e.g., plagiogranites).

Petrogenetic model

As a simplifying assumption, and summarised in Fig. 10, we postulate that most of the IC, while thicker and more heterogeneous, is geochemically and compositionally similar to the typical oceanic crust for most of Iceland (Mutter and Mutter 1993; Darbyshire et al. 2000; Foulger et al. 2003), containing layers of gabbro and basalts derived by partial melting from a depleted source. Pockets of plagiogranite are assumed to occur sparsely in the boundary between gabbro layers and basalts (Sigurdsson 1977; Foulger et al. 2003), derived by fractional crystallisation from basaltic melts, and contain relatively low incompatible element concentrations. These pockets are intruded by rising basaltic melt, either from partial melting of the depleted mantle, within active rift zones (Mælifell, Ketilhyrnur and Prestahnúkur) or from greater depths, associated with a mantle plume within flank regions (e.g., Sultarfell). The intrusions of magma promote the partial melting of these plagiogranite pockets, due to its lower melting point compared to surrounding lithologies Volume constraints preclude this mechanism to generate all Icelandic rhyolites, but it is adequate for the smaller HSR rhyolitic bodies not associated with a CV, studied here.

Partial melting models of plagiogranites using rhyolite-MELTS produce compositions with ~ 76–82 wt% SiO_2,

while trace element calculations based on their content in the plagiogranite reproduce closely the concentration of Rb, Y and Ba found in the HSR (Table 8). Zr and Nb are depleted in the generated melt as their host minerals (e.g., zircon and ilmenite) remain in the plagiogranite restite. Variations in Sr content is likely consequence of an additional mechanism of plagioclase crystallisation and fractionation likely prior magma ascent.

Once the HSR melt is generated, being less dense than the surrounding IC, and comparatively more buoyant than the basaltic melt, it rises relatively fast, experiencing adiabatic decompression and low nucleation and low diffusion rates, likely inhibiting crystallization. This is consistent with recent evidence for rapid ascent ($0.5\,m{\cdot}s^{-1}$) of near-aphyric HSR at Chaitén, Chile in 2008 (Castro and Dingwell; 2009; Wicks et al. 2011), via a dyke pathway from storage at ~ 5 km depth.

As these are relatively dry magmas, their viscosity is higher (~ 10^7 Pa s based on sample PK1 composition calculated using rhyolite-MELTS at 100 MPa and the liquidus temperature) than more water-rich HSR melts generated from other intrusive bodies (e.g., ~ $10^{4.5}$ Pa s inferred viscosity of residual melts from granites at later stages of crystallisation; Bachmann and Bergantz 2004). We propose that this relatively higher viscosity hinders crystal-melt separation during ascent, perhaps promoting some transport, albeit minimal, of a plagiogranite-derived mineralogy (e.g., allanite, and zircon phenocrysts, all mineral phases found in oceanic plagiogranites; Anenburg et al. 2015), or crystals from a crystal mush zone. Alternatively, some phases may represent minor crystallising phases (fayalite, hedenbergite, quartz).

Conclusions

Our results demonstrate that HSRs in Iceland can be generated either by fractional crystallisation and decompression to shallow conditions, or by the partial melting of likely plagiogranites generated by fractional crystallisation of basaltic melts in the IC. However, based on trace element content, crystal cargo and the lack of a long-lived magmatic system to ensure shallow conditions and a hydrothermal system, we favour the partial melting model to generate the studied HSRs presented here.

These results extend our knowledge and understanding of the compositional diversity and complexity of origin of evolved magmas in the Icelandic crust and emphasise the continued need to further investigate the relevant roles of partial melting and fractional crystallisation in the generation of evolved compositions.

Supplementary Information The online version contains supplementary material available at https://doi.org/10.1007/s00710-026-00993-x.

Acknowledgements The authors of this contribution wish to acknowledge The Open University and the University of Leicester for the whole-rock chemical analyses and The Open University for the Mineral Chemistry analyses used in this work. Hugh Tuffen was supported by a Royal Society University Research Fellowship. We thank the reviews of two anonymous reviewers and the editors of the journal for thorough reviews and suggestions, which greatly improved the manuscript.

Author contributions All authors contributed to the writing and reviewing of the manuscript. AH & JC performed all geochemical modelling, and prepared all figures. DMG & AT completed sample collection and analysis.

References

Ando A (1984) New silicate rock reference materials issued from the Geological Survey of Japan. Geochem J 18(4):215–216

Anenburg M, Katzir Y, Rhede D, Jöns N, Bach W (2015) Rare earth element evolution and migration in plagiogranites: a record preserved in epidote and allanite of the Troodos ophiolite. Contrib Mineral Petrol 169:1–19

Asimow PD, Ghiorso MS (1998) Algorithmic modifications extending MELTS to calculate subsolidus phase relations. Am Mineral 83:1127–1131

Bachmann O, Bergantz GW (2004) On the origin of crystal-poor rhyolites: extracted from batholithic crystal mushes. J Petrol 45:1565–1582

Bacon CR, MacDonald R, Smith RL, Baedecker PA (1981) Pleistocene high silica rhyolites of the Coso volcanic field, Inyo County, California. J Geophys Res 86(B11):10223–10241

Bartels A, Behrens H, Holtz F, Schmidt BC, Fechtelkord M, Knipping J, Crede L, Baasner A, Pukallus N (2013) The effect of fluorine, boron and phosphorus on the viscosity of pegmatite forming melts. Chem Geol 346:184–198

Blundy J, Cashman K (2001) Ascent-driven crystallisation of dacite magmas at Mount St Helens, 1980–1986. Contrib Mineral Petrol 140:631–650

Bowen NL (1921) Diffusion in silicate melts. J Geol 29(4):295–317

Brill RH (1999) Chemical analyses of early glasses. Tables of Analyses, The Corning Museum of Glass, Corning 2

Buddington AF, Lindsley D (1964) Iron-titanium oxide minerals and synthetic equivalents. J Petrol 5:310–357

Bunsen RW (1851) Uber die processe der vulkanischen Gesteinsbildungen Islands. Ann Phys Chem (Dritte Reihe) 83:197–272

Butterman WC, Foster WR (1967) Zircon stability and the ZrO_2-SiO_2 phase diagram. Am Mineral 52:880–885

Carmichael ISE (1964) The petrology of Thingmúli, a tertiary volcano in eastern Iceland. J Petrol 5(3):435–460

Castro JM, Dingwell DB (2009) Rapid ascent of rhyolitic magma at Chaitén Volcano, Chile. Nature 461(7265):780–783

Charreteur G, Tegner C, Haase K (2013) Multiple ways of producing intermediate and silicic rocks within Thingmúli and other Icelandic volcanoes. Contrib Mineral Petrol 166:471–490

Coleman RG, Donato MM (1979) Chapter 5. Oceanic plagiogranite revisited. In: Barker F (edr): Developments in Petrology 6:149–168 https://doi.org/10.1016/B978-0-444-41765-7.50010-1

Coleman RG, Peterman ZE (1975) Oceanic plagiogranite. J Geophys Res 80:1099–1108

Cortés JA, Wilson M, Condliffe E, Francalanci L (2006) The occurrence of forsterite and highly oxidising conditions in basaltic lavas from Stromboli Volcano, Italy. J Petrol 47:1345–1373

Darbyshire FA, White RS, Priestley KF (2000) Structure of the crust and uppermost mantle of Iceland from a combined seismic and gravity study. Earth Planet Sci Lett 181:409–428

Deer WA, Howie RA, Zussman J (2013) An introduction to the rock forming minerals, 3rd excerpted student's Edition. Mineralogical Society, London, p 498

Deering CD, Cole JW, Vogel TA (2008) A rhyolite compositional continuum governed by lower crustal source conditions in the Taupo Volcanic Zone, New Zealand. J Petrol 49:2245–2276

Duggan MB (1976) Primary allanite in vitrophyric rhyolites from the Tweed Shield Volcano, north-eastern New South Wales. Mineral Mag 40(314):652–653

Einarsson P, Sæmundsson K, (1987) Earthquake epicenters 1982–1985 and volcanic systems in Iceland: A map, in Í hlutarins eðli, Festschrift for Þorbjörn Sigurgeirsson, edited by Sigfússon, Menningarsjóður. Reykjavík

Elders WA, Friðleifsson GÓ, Zirenberg RA, Pope EC, Mortensen AK, Guðmundsson A, Lowenstern JB, Marks NE, Owens L, Bird DK, Reed M, Olsen NJ, Schiffman P (2011) Origin of a rhyolite that intruded a geothermal well while drilling at the Krafla volcano, Iceland. Geology 39:231–234

Evans OC, Hanson GN (1993) Accessory-mineral fractionation of rare-earth elements (REE) abundances in granitoid rocks. Chem Geol 110:69–93

Floyd PA, Yaliniz MK, Goncuoglu MC (1998) Geochemistry and petrogenesis of intrusive and extrusive ophiolitic plagiogranites, Central Anatolian Crystalline Complex, Turkey. Lithos 42:225–241

Flude S, McGarvie DW, Burgess R, Tindle AG (2010) Rhyolites at Kerlingarfjöll, Iceland: the evolution and lifespan of silicic central volcanoes. Bull Volcanol 72:523–538

Foulger GR, Anderson DL (2005) A cool model for the Iceland hotspot. J Volcanol Geotherm Res 141:1–22

Foulger GR, Du Z, Julian BR (2003) Icelandic- type crust. Geophys J Int 155:567–590

Friðleifsson GÓ, Elders WA, Albertsson A (2014) The concept of the Iceland deep drilling project. Geothermics 49:2–8

Friðleifsson GÓ, Elders WA, Zierenberg RA, Fowler AP, Weisenberger TB, Mesfin KG, Sigurðsson Ó, Níelsson S, Einarsson G, Óskarsson F, Guðnason EÁ (2020) The Iceland deep drilling project at Reykjanes: drilling into the root zone of a black smoker analog. J Volcanol Geotherm Res 391:106435

Gamal El Dien H, Li ZX, Abu Anbar M, Doucet LS, Murphy JB, Evans N, Xia XP, Li J (2021) The largest plagiogranite on earth formed by re-melting of juvenile proto-continental crust. Commun Earth Environ 2:1–16

Gerlach DC, Leeman WP, Avé Lallemant HG (1981) Petrology and geochemistry of plagiogranite in the Canyon Mountain Ophiolite, Oregon. Contrib Mineral Petrol 77:82–92

Ghiorso MS, Sack RO (1995) Chemical mass transfer in magmatic processes. IV. A revised and internally consistent thermodynamic model for the interpolation and extrapolation of liquid-solid equilibria in magmatic systems at elevated temperatures. Contrib Mineral Petrol 119:197–212

Ghiorso MS, Stolper EM (1999) Calculation of peridotite partial melting from thermodynamic models of minerals and melts. II. Isobaric variations in melts near the solidus and owing to variable source composition. J Petrol 40:297–313

Gladney ES, Roelandts I (1988) Compilation of elemental concentration data for USGS BHVO-1, MAG-1, QLO-1, RGM-1, SCo-1, SDC-1, SGR-1, and STM-1. Geostand Newsl 12:253–362

Gladney ES, Roelandts I (1990) Compilation of elemental concentration data for CCRMP reference rock samples SY-2, SY-3 and MRG-1. Geostand Newsl 14:373–458

Glazner AF, Coleman DS, Bartley JM (2008) The tenuous connection between high silica rhyolites and granodiorite plutons. Geol Soc Am Bull 36:183–186

Gualda GAR, Ghiorso MS (2013) Low pressure origin of high-silica rhyolites and granites. J Geol 121:537–545

Gualda GAR, Ghiorso MS, Lemons RV, Carley TL (2012) A modified calibration of MELTS optimised for silica-rich, fluid bearing magmatic systems. J Petrol 53:875–890

Gudmundsson A (1995) Infrastructure and mechanics of volcanic systems in Iceland. J Volcanol Geotherm Res 64(1–2):1–22

Gurenko AA, Sobolev AV (2006) Crust–primitive magma interaction beneath neovolcanic rift zone of Iceland recorded in gabbro xenoliths from Midfell, SW Iceland. Contrib Mineral Petrol 151(5):495–520

Henderson J (1988) Electron-microprobe investigation of early Irish glass and glass-making practices. MSR Online Proc Libr 123:141–146

Hughes A, Cortés JA, McGarvie D, Moscati RJ, Olive V (2026) The petrogenesis of Þingmúli volcano, East Fjords, Iceland. J Volcanol Geotherm Res 472:108561

Irvine TN, Baragar WRA (1971) A guide to the chemical classification of the common volcanic rocks. Can J Earth Sci 8:523–548

Jin X, Han J (2011) K-Medoids Clustering. In: Sammut, C., Webb, G.I. (eds) Encyclopedia of Machine Learning. Springer, Boston, MA https://doi.org/10.1007/978-0-387-30164-8_426

Jónasson K (2007) Silicic volcanism in Iceland: composition and distribution within the active volcanic zones. J Geodyn 43:101–117

Jónasson K, Holm PM, Pedersen AK (1992) Petrogenesis of silicic rocks from the Kroksfjordur central volcano NW Iceland. J Petrol 33:1345–1369

Kirkpatrick RJ (1983) Theory of nucleation in silicate melts. Am Mineral 68:66–77

Lacasse C, Sigurdsson H, Carey SN, Jóhannesson H, Thomas LE, Rogers NW (2007) Bimodal volcanism at the Katla subglacial caldera, Iceland: insight into the geochemistry and petrogenesis of rhyolitic magmas. Bull Volcanol 69:373–399

Lambert IB, Wyllie PJ (1972) Melting of a gabbro (quartz eclogite) with excess water to 35 kilobars, with geological applications. J Geol 80:693–708

Lawver LA, Müller RD (1994) Iceland hotspot track. Geology 22:311–314

Le Maitre RW, Streckeisen A, Zanettin B, Le Bas MJ, Bonin B, Bateman P (2002) Igneous Rocks: A Classification and Glossary of Terms: Recommendations of the International Union of Geological Sciences Subcommission on the Systematics of Igneous Rocks, 2nd ed. Cambridge University Press. https://doi.org/10.1017/CBO9780511535581

Lee C-T, Morton DM (2015) High silica granites: terminal porosity and crystal settling in shallow magma chambers. Earth Planet Sci Lett 409:23–31

Lehnert K, Su Y, Langmuir CH, Sarbas B, Nohl U (2000) A global geochemical database structure for rocks. Geochem Geophys Geosyst 1:1012

Lowenstern JB, Mahood GA (1991) Petrogenesis of high silica rhyolite on the Alaska Peninsula. Geophys Res Lett 18:1565–1568

MacDonald R, Davies GR, Bliss CM, Leat PT, Bailey DK, Smith RL (1987) Geochemistry of high-silica peralkaline rhyolites Naivasha Kenya Rift Valley. J Petrol 28:979–1008

MacDonald R, McGarvie DW, Pinkerton H, Smith RL, Palacz ZA (1990) Petrogenetic evolution of the Torfajökull volcanic complex, Iceland: I. relationships between the magma types. J Petrol 31:429–459

Martin E, Sigmarsson O (2007) Crustal thermal state and origin of silicic magma in Iceland: the case of Torfajökull, Ljósufjöll and Snæfellsjökull volcanoes. Contrib Mineral Petrol 153(5):593–605

Masotta M, Mollo S, Nazzari M, Tecchiato V, Scarlato P, Papale P, Bachmann O (2018) Crystallization and partial melting of rhyolite and felsite rocks at Krafla volcano: a comparative approach based on mineral and glass chemistry of natural and experimental products. Chem Geol 483:603–618

McGarvie DW, MacDonald R, Pinkerton H, Smith RL (1990) Petrogenetic evolution of the Torfajökull volcanic complex, Iceland II. The role of magma mixing. J Petrol 31(2):461–481

McGarvie DW, Stevenson JA, Burgess R, Tuffen H, Tindle AG (2007) Volcano-ice interactions at Prestahnúkur, Iceland: Rhyolite eruption during the last interglacial-glacial transition. Ann Glaciol 45:38–47

Meek a, Henderson J, Evans J (2012) Isotope analysis of English forest glass from the Weald and Staffordshire. J Anal At Spectrom 27:786

Miller CF, Mittlefehldt DW (1984) Extreme fractionation in felsic magma chambers: A product of liquid-state diffusion or fractional crystallization? Earth Planet Sci Lett 68:151–158

Mutter CZ, Mutter JC (1993) Variations in thickness of layer 3 dominate oceanic crustal structure. Earth Planet Sci Lett 117:295–317

Oziegbe EJ, Ocan OO, Buraimoh AO (2020) Petrography of allanite-bearing tonalite from Iwo region, Osun state, Nigeria. Mater Geoenvironment. https://doi.org/10.2478/rmzmag-2020-0006

Papike JJ, Cameron KL, Baldwin K (1974) Amphiboles and pyroxenes: Characterization of other than quadrilateral components and estimates of ferric iron from microprobe data. Geol Soc Am Abstr Programs 6:1053–1054

Pouchou JL, Pichoir F (1991) Quantitative analysis of homogeneous or stratified microvolumes applying the model 'PAP.' In: Heinrich KFJ, Newbury DE (eds) Electron Probe Quantitation. Plenum Press/Springer, New York, pp 31–75. https://doi.org/10.1007/978-1-4899-2617-3-4

Putirka K (2008) Thermometers and barometers for volcanic systems. Rev Mineral Geochem 69:61–120

Reed SJB, Buckley A (2018) Rare-earth element determination in minerals by electron-probe microanalysis: application of spectrum synthesis. Mineral Mag 62:1–8

Roeder PL, Emslie RF (1970) Olivine-liquid equilibrium. Contrib Mineral Petrol 29:275–289

Rollinson H (2009) New models for the genesis of plagiogranites in the Oman ophiolite. Lithos 112:603–614

Saubin E, Kennedy B, Tuffen H, Nichols AR, Villeneuve M, Bindeman I, Mortensen A, Schipper CI, Wadsworth FB, Watson T, Zierenberg R (2021) Textural and geochemical window into the IDDP-1 rhyolitic melt, Krafla, Iceland, and its reaction to drilling. GSA Bull 133(9–10):1815–1830

Schmincke HU, Viereck LG (1982) Volcaniclastic rocks of the Reydarfjördur drill hole, Eastern Iceland. 1. Primary features. J Geophys Res Solid Earth 87(B8):6437–6458

Sigurdsson H (1977) Generation of Icelandic rhyolites by melting of plagiogranites in the ocean layer. Nature 269:25–28

Smith PM, Asimow PD (2005) Adiabat_1ph: a new public front-end to the MELTS, pMELTS, and pHMELTS models. Geochem Geophys Geosyst. https://doi.org/10.1029/2004GC000816

Streck MJ (2002) Partial melting to produce high-silica rhyolites of a young bimodal suite: compositional constraints among rhyolites, basalts and metamorphic xenoliths from the Harney Basin, Oregon. Int J Earth Sci 91:583–593

Streck MJ, Grunder AL (1997) Compositional gradients and gaps in high silica rhyolites of the Rattlesnake Tuff Oregon. J Petrol 38:133–163

Thordarson T, Larsen G (2007) Volcanism in Iceland in historical times: volcano types, eruption styles and eruptive history. J Geodyn 43:118–152

Tindle AG (2008) Minerals of Britain and Ireland. Terra Publishing, London, p 624p

Tuffen H, Castro JM (2009) The emplacement of an obsidian dyke through thin ice: Hrafntinnuhryggur, Krafla Iceland. J Volcanol Geotherm Res 185(4):352–366

Tuttle OF, Bowen NL (1958) Origin of granite in the light of experimental studies in the system NaAlSi3O8–KAlSi3O8–SiO_2–H_2O. Geol Soc Am Mem 74:153

Walker GPL (1966) Acid volcanic rocks in Iceland. Bull Volcanol 29(1):375–402

Whitney DL, Evans BW (2010) Abbreviations for names of rock-forming minerals. Am Mineral 95(2):185–218

Wicks C, de La Llera JC, Lara LE, Lowenstern J (2011) The role of dyking and fault control in the rapid onset of eruption at Chaitén volcano, Chile. Nature 478(7369):374–377

Wolff JA, Ramos FC (2015) Processes in caldera-forming high silica rhyolite magma: Rb-Sr and Pb isotope, systematics of the Otowi member of the Bandlier tuff, Valles caldera, New Mexico, USA. J Petrol 55:345–375

Yakymchuk C, Brown M (2014) Behaviour of zircon and monazite during crustal melting. J Geol Soc 171:465–479

Zhang JH, Yang JH, Chen JY, Wu FY, Wilde SA (2018) Genesis of late Early Cretaceous high silica rhyolites in eastern Zhejiang province, southeast China: a crystal mush origin with mantle input. Lithos 296:482–495

Zierenberg RA, Fowler AP, Friðleifsson GÓ, Elders WA, Weisenberger TB (2017) Preliminary description of rocks and alteration in IDDP-2 drill core samples recovered from the Reykjanes geothermal system, Iceland. GRC Trans 41:1599–1615

Zincone SA, Oliveria EP, Laurent O, Zhang H, Zhai M (2016) 3.30 Ga high-silica intraplate volcanic–plutonic system of the Gavião Block, São Francisco craton, Brazil: evidence of an intracontinental rift following the creation of insulating continental crust. Lithos 266:414–343